ACS OMEGA

Article

Cite This: ACS Omega 2019, 4, 4129−4137

http://pubs.acs.org/journal/acsodf

High-Loading Carbon Nanotubes on Polymer Nanofibers as Stand-Alone Anode Materials for Li-Ion Batteries

Alan Christian Lim,[†,§] Harsharaj S. Jadhav,[†,§] Hyuk Jae Kwon,[‡] and Jeong Gil Seo*[,†]

[†]Department of Energy Science and Technology, Myongji University, 116 Myongji-ro, Cheoin-gu, Yongin-si, Gyeonggi-do 17058, Republic of Korea

[‡]Samsung Advanced Institute of Technology, Samsung Electronics, Company Limited, 130 Samsung-ro, Yeongtong-gu, Suwon-si, Gyeonggi-do 16678, Republic of Korea

Supporting Information

ABSTRACT: To address the instability and repulsive interaction of carbon nanotubes (CNTs) in Li-ion batteries, mixed polymers (polyacrylonitrile and polyvinylpyrrolidone) were employed as matrix support to ensure that CNT particles remain in place during charge/discharge process and prevent particle migration. Various CNT-based anodes have been reported, but these require metal support that could result in contact resistance. Hence, free-standing CNT electrodes are an attractive option. A simple method of electrospinning polymers and calcination at 800 °C is presented with CNT loading as high as 50 wt % can be obtained without binder and acts as main active material rather than an additive as described in previous studies. The anode [pyrolyzed polymer (PP)-CNT] showed excellent performance with a high discharge specific capacity of 960 mA h/g at a current density of 200 mA/g. The capacity at a higher current density (1600 mA/g) remained greater than graphite (372 mA h/g) at 521 mA h/g and showed a high stability for 675 cycles without exhibiting any significant capacity loss with a Coulombic efficiency of >95%. A rate capability experiment showed the reversibility of PP-CNTs after subjecting them to an increasing current density and regaining >95% of the initial capacity at a low current density (200 mA/g). The high capacitive performance of the material is attributed to the high loading of CNTs and their containment within the bulk of the polymer matrix to prevent particle migration and agglomeration as well as the capacity of the nanofibers to preserve a tight proximity of the electrolyte−electrode interface.

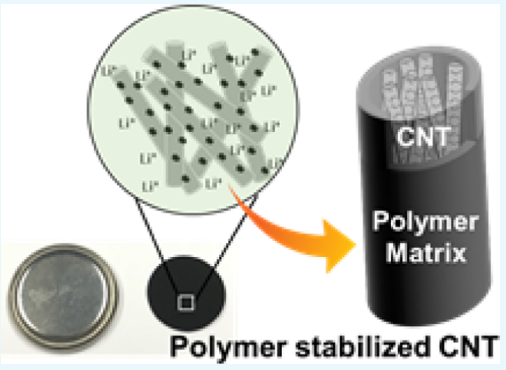

INTRODUCTION

Energy storage devices have emerged as the current leading breakthrough for alternative technology to the traditional rechargeable batteries such as lead−acid batteries, nickel−cadmium batteries, and nickel−metal hydride batteries.[1−3] Most of the electronic devices nowadays use Li-ion batteries (LIBs) to power a wide range of portable devices such as cell phones, laptops, digital cameras, and so on.[4−6] The surge of interest to develop electrode material has paved the way to consider LIBs as a secondary power unit to electronic vehicles to replace fossil fuel-based energy.[7] Graphite has been widely used commercially as it is relatively cheap, readily available, and has a long lifespan. However, graphite has a very limited capacity of 372 mA h/g, which limits its application, which requires a higher capacity.[8−10]

To meet the increasing demand for energy, considerable efforts have been made to study different kinds of anode materials. Among the potential candidates, the most widely explored materials for LIBs are graphene, carbon nanotubes (CNTs), hierarchically porous carbon, hollow carbon nanospheres, and so on.[11−16] Among the materials mentioned, CNTs present unique and attractive benefits as an active material. In comparison to graphite, they can significantly increase the specific capacity without suffering from pulverization because of their mechanical stability. They also offer a unique structure (one-dimensional cylindrical tube) as a support for composite materials, high conductivity, and relative inertness, which are highly attractive characteristics for an anode material from a practical point of view.[17]

Recently reported studies showed utilization of CNTs both as a support and main component for anode materials. Lin et al. synthesized a nano-$TiNb_2O_7$/CNT composite with a specific capacity of 346 mA h/g at 0.1 C and 163 mA h/g at a high C-rate (30 C) with a fairly simple synthesis method.[18] Although the anode material presents a facile synthesis, it requires the usage of highly toxic chemicals such as acid treatments on CNTs. Consequently, it can change the intrinsic properties of CNTs and form unnecessary and uncontrollable defects. On the other hand, Zhao et al. reported an in situ growth amorphous CNT on a Si particle via chemical vapor deposition.[19] The reported capacity is 1496 mA h/g at 100 mA/g, but reversible capacity can only retain 80% of its

Received: November 4, 2018
Accepted: January 18, 2019
Published: February 25, 2019

DOI: 10.1021/acsomega.8b03073
ACS Omega 2019, 4, 4129−4137

Scheme 1. Schematic Representation of the Fabrication of Polymer Fiber Composite

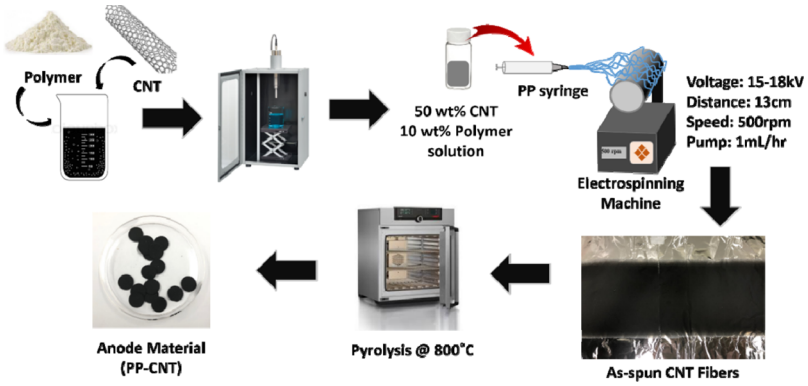

original capacitance after 300 cycles. Aside from being used as an additive, CNT as a sole anode material has also been widely explored. Di Lecce et al. report the use of a multiwalled CNT against three different kinds of cathode materials. However, because of CNT's powder nature, it requires to be cast onto a metal foil as support together with different materials such as binder, which can result in an increase in contact resistance.[20] With the increase in the number of components arises different types of material interfaces that can heavily impact the overall internal resistance of LIBs.[21] Therefore, developing a free-standing electrode system is highly required to reduce the interfaces between grains of active material and present an easier fabrication method.

In this study, facile fabrication of an electrospun polymer nanofiber with a CNT loading amounting up to 50 wt % (based on the polymer amount) has been presented. This high loading was made possible by using two kinds of polymer to control the viscosity of the polymer solution. This polymer matrix serves as a porous support to the CNT during the charge/discharge process to prevent any type of movement or migration as well as an electrolyte reservoir. In addition, this polymer matrix also serves to hold the electrode material and render the fabricated polymer nanofiber as a freestanding anode material. This fabrication method is not only limited to the LIB application but could also find potential benefits in other storage applications such as sodium and potassium batteries where liquid electrolyte is highly beneficial.[22−24] The electrode material can absorb the electrolyte and maintain a good electrode−electrolyte contact, promoting the conduction of ions, especially for all-solid-state systems. Pyrolyzed polymer (PP)-CNTs calcined at 800 °C showed excellent performance at a current density of 200 mA/g with a lithium storage capacity of 960 mA h/g after 500 cycles and maintained a Coulombic efficiency of ∼97−99%. At a high current density of 1600 mA/g, the capacitance remained higher than that of graphite (372 mA h/g), recording a value at 521 mA h/g, which is an outstanding performance and reproduced 95% of the original capacitance of 915 mA h/g, indicating its excellent rate capability.

RESULTS AND DISCUSSION

Preparing the Anode Material. The preparation of the electrode material is illustrated in Scheme 1. In lieu of fabricating a high loading CNT polymer nanofiber, the CNT should be properly dispersed to guarantee good distribution throughout the bulk of the nanofibers. This also prevents the possibility of forming large particles that could disrupt the flow of the polymer solution during the electrospinning process.[25] Thus, in order to fabricate the polymer fiber, the CNTs were finely ground and sieved to selectively filter out the larger-sized particles and use only fine powders to create the suspension to ensure a well-dispersed solution. *N*,*N*′-Dimethylformamide (DMF), commonly used in combination to make a CNT suspension, was chosen as the main solvent. It can also dissolve both polyacrylonitrile (PAN) and polyvinylpyrrolidone (PVP), easily making it the ideal choice. Before adding the polymers, the DMF solution of CNTs was ultrasonicated to enhance the dispersion in the solution. Both PAN and PVP were added and stirred overnight to allow proper mixing of the polymers and the CNTs. Utilizing PAN and PVP was integral in achieving high CNT loading in the as-spun polymer nanofiber. A minimum requirement of at least 10 wt % polymer is necessary to electrospin a decent amount of CNT loading (∼20 wt % CNT, based on polymer amount). However, above 20 wt % CNT, the PAN solution tends to become too viscous to be electrospun when utilized alone. PAN, as a support, presents an advantage because it is considered as the polymer that has the highest carbon yield after thermal treatment as compared to other polymers.[26,27] It will result in better stability as a matrix support for the CNT after pyrolysis. If the carbon yield is too low, the integrity of holding the CNT particles inside can be compromised and could lead to most of the CNT particles falling out of the polymer matrix after heat treatment. Moreover, the nanofiber morphology might not even form if there is a very low carbon yield. Thus, it is important to choose an appropriate temperature. Hence, 800 °C was chosen for the thermal treatment to balance the trade-off between conductivity and carbon yield.[28] In order to circumvent the viscosity issue, a mixed polymer (PAN and PVP) was used to decrease the viscosity and yet maintain the polymer weight loading at 10 wt %. Using the optimum weight ratio (1:1), a high CNT loading (50 wt %) polymer nanofiber was obtained. Shown in Scheme S1 is an example image of the freestanding electrodes with PP-CNT acting as the main anode material, and without CNT loading (PP), which will be used as the control for performance comparison. Decreasing the amount of PAN below 1:1 renders the polymer fiber too weak to hold its form and it will not be successfully electrospun.

Figure 1a,b shows the nanofiber morphology of the as-spun polymer nanofibers and heat-treated polymer nanofibers at 800 °C. It can be seen that the material retained its structure after pyrolysis and contains a similar appearance to the as-spun nanofibers. Large CNT particles were still present but most of them were fixed within the nanofiber matrix as observed in the

DOI: 10.1021/acsomega.8b03073
ACS Omega 2019, 4, 4129−4137

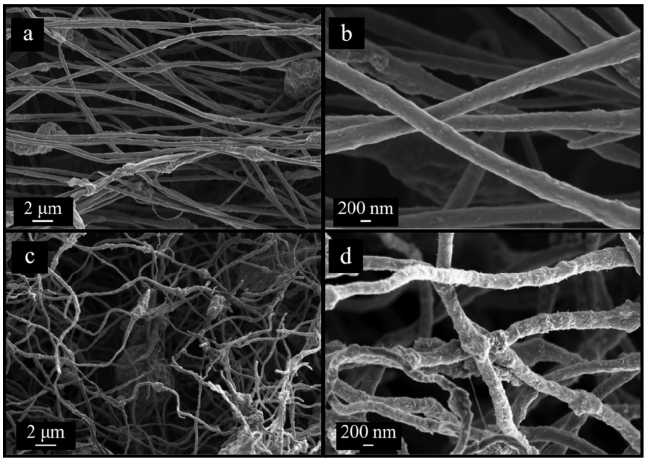

Figure 1. FE-SEM images of (a,b) as-spun PAN-PVP-CNT and (c,d) pyrolyzed PP-CNT nanofibers.

low magnification images. Also, a few large CNT particles can be observed located in the external matrix of the polymer nanofiber. These can still be stabilized by the polymer nanofiber through the interpore formed by intersecting polymer fibers around the large CNT particle. After heat treatment, the PP-CNT was obtained and exhibits the same morphology (Figure 1c,d). At a higher magnification (Figure S1), the surface of the nanofiber exhibits a difference in contrast in certain areas with bright spots throughout the entire fiber. Indicated in red circles, these are the individual CNT strands that are protruding and extending outward from the surface of the carbon matrix. This can be observed throughout the surface of all the fibers, which indicates that there is an even distribution of the CNTs, hence successfully embedding the high amount of CNTs inside. The exposed strands can result in an enhancement of the performance of the material because of a more direct contact with the electrolyte solution as compared to the CNT inside the polymer matrix. It can also prove beneficial where the initial Li^+ intercalation can occur through the exposed strands and the lithium ion can migrate easier into the bulk.

TEM images shown in Figure S2a,b further support the successful embedding of CNT particles inside the polymer matrix. At a low magnification, CNT strands can be seen occupying the inner portion of the polymer matrix at the edge of the nanofiber. Moreover, Figure S2b clearly shows from a cross-sectionally broken CNT-polymer nanofiber that several CNT strands are protruding out from the center of the material. This observation, together with the scanning electron microscopy (SEM) images, defines and supports the claim that the CNTs are bound within the structural framework provided by the nanofiber, creating a mechanical stabilizer that prevents any type of CNT movement under bias.

To establish the presence of CNTs in the polymer nanofiber, different spectroscopic analyses were employed. The anode material was analyzed with Fourier-transform infrared spectroscopy (FT-IR) (Figure 2a) to show characteristic peaks of PAN at ∼2240, ∼2930, and ∼1453 cm^{-1} for the nitrile group (−C≡N) and stretching and bending vibration of the methylene group (=C−H), respectively.[29] PVP also showed distinct peaks such as hydroxyl groups (−OH) with a strong broad peak at ∼3406 cm^{-1}, and the methylene group (=C−H) and the carboxyl group (−C=O) at 1647 cm^{-1}.[30] All these

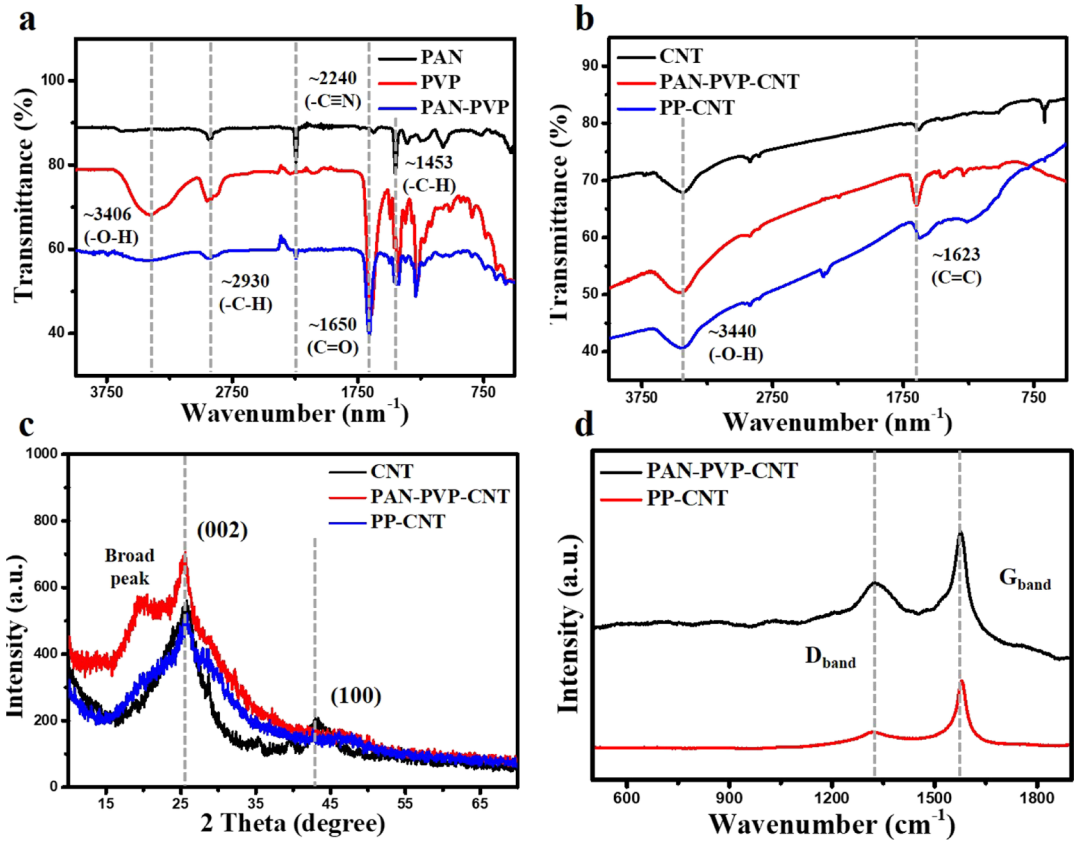

Figure 2. Spectroscopic analysis of bare polymer nanofiber and PP-CNT using (a,b), FT-IR, (c) XRD, and (d) Raman analysis.

DOI: 10.1021/acsomega.8b03073
ACS Omega 2019, 4, 4129−4137

functionalities are evidently present in the as-spun PP-CNTs, which proves that the mixed polymer nanofiber is successfully fabricated. In addition, the FT-IR spectrum (Figure 2b) of CNT, PAN-PVP-CNT, and PP-CNT electrodes shows a very similar IR spectrum compared with the pristine CNT, indicating the preserved features and presence of the CNT within the material. The peaks corresponding to the polymer fibers disappeared after calcination and only a strong broad peak and sharp peak at ∼3440 for hydroxyl groups and ∼1623 cm^{-1} for conjugated carbon (C═C) was observed. X-ray diffraction (XRD) analysis (Figure 2c) shows the crystallinity of CNT by the presence of the peaks corresponding to the (002) and (100) phases both in the pristine CNT and the PAN-PVP-CNT. These peaks, in lower intensity, still remained even before and after calcination as evidenced by the observed peak at ∼25° and a broader peak at ∼43°.[31] The broad peak for the PAN-PVP-CNT at ∼19° can be attributed to the polymer nanofiber, which is evidently shown in Figure S3 wherein only amorphous phases of the polymer nanofibers are present in the spectra of all the samples. This amorphous peak, however, disappears because of its transformation to graphitized carbon species after calcination.[32,33] Figure 2d presents the Raman spectra of PAN-PVP-CNT and PP-CNT. Two distinct peaks were observed at around ∼1320 and 1581 cm^{-1} that are assigned to D and G bands, respectively. The G band is associated with the highly ordered and graphitized carbons with an sp^2 hybridization. On the other hand, the D band is normally associated with defects and disordered carbons and the intensity of these two bands reflect the amount of graphitization, hence the degree of conductivity of a carbon material.[34,35] The I_D/I_G ratio of the as-spun PP-CNT decreased from 0.93 to 0.70 (PP-CNT), indicating that more graphitized carbon species were introduced on the surface as a result of carbonization.[36,37]

The Brunner−Emmet−Teller (BET) surface area and porosity of CNT and PP-CNT were characterized by N_2 adsorption−desorption isotherm measurements at 77 K, as shown in Figure 3a,b, respectively. The isotherm of both samples belongs to type IV with a hysteresis loop (according to the International Union of Pure and Applied Chemistry (IUPAC) classification), indicating its mesoporous structure as evidenced also in Figure 3b. The pore size distribution curve for PP-CNTs showed a peak and a slight shouldering at around ∼17 and ∼28 nm attributed to the presence of CNTs within the nanofiber. As the CNTs were embedded, the intensity of the peaks was expected to diminish not because of structural changes and deformation but because of lower accessibility to the pore structure of CNTs in PP-CNTs as compared to the pristine CNTs. The recorded surface areas of CNTs and PP-CNTs were 582 and 388 m^2/g, respectively. The recorded pore volumes were 2.41 and 0.701 with an average pore diameter of 16.5 and 12.7 both for CNTs and PP-CNTs. Although the surface area and the pore volume decreased, fixing the CNTs in place will prevent the migration of the particles and prevent repulsive interaction of adjacent CNT particles during the charge/discharge process. Formation of agglomerated particles is unfavorable in the LIB system because larger particles have a lower surface area in contact with the electrolyte regardless of the amount of loading. This leads to a low discharge capacity or can also render them highly inactive material because most of the CNTs in the bulk do not have a direct interaction with the electrolyte solution. Smaller particles will have a higher surface area to electrolyte ratio and will be able to maximize the amount of CNTs in the anode material. The presence of the polymer matrix will also act as an electrolyte pool or reservoir to maintain a tight proximity of the electrolyte (Li^+ ions) and the CNT particles. Moreover, better ion diffusion can be expected because of the porous nature of the PP nanofiber.

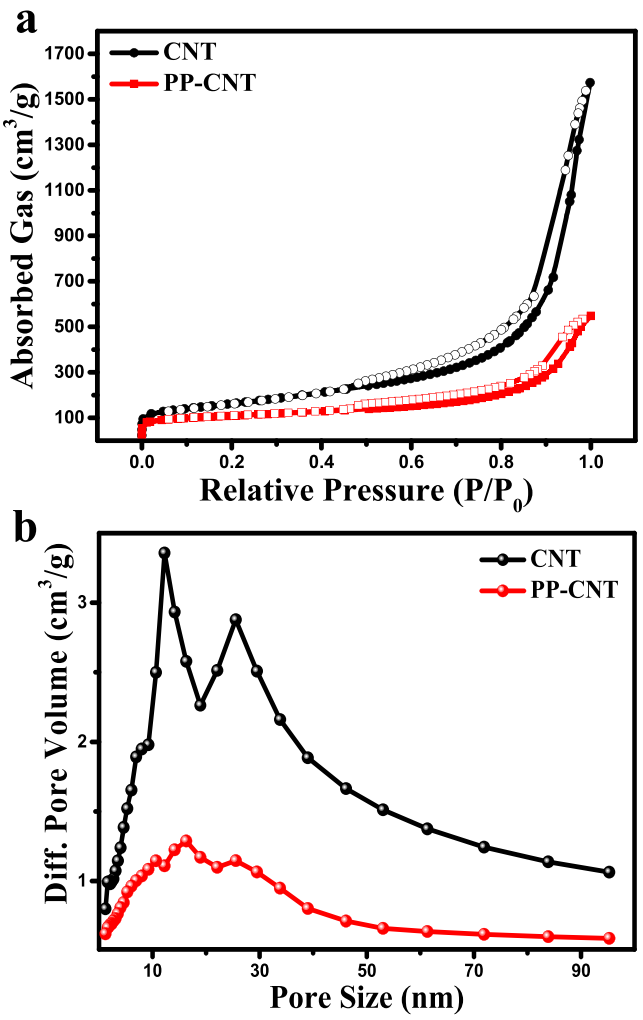

Figure 3. (a) Nitrogen adsorption/desorption isotherm curves and (b) pore size distribution curve for a CNT and a PP-CNT recorded at 77 K.

Electrochemical Measurement. Initially, the as-spun polymer fibers were used as anode material without heat treatment. The data are presented in Figure S5 where the performance is compared to PP-CNTs after pyrolysis. Because of the nature of polymers as an insulating material, no significant activity was observed during the charge/discharge process. The untreated polymer layer passivated the CNT particles and did not exhibit good conductance. Thus, the thermal treatment of the polymer fiber was proven integral to render the polymer nanofiber a highly conductive layer, resulting in a high-performance electrode. The polymer nanofiber was first stabilized at 280 °C to stabilize and convert the carbon skeleton into a graphitic-like structure and then increased the temperature to 800 °C to improve its porosity and surface area because of the transformation of the carbon skeleton of PAN into graphitic carbon and this is a widely established concept for carbon material. Temperature for the heat treatment is a crucial factor because it will dictate the

DOI: 10.1021/acsomega.8b03073
ACS Omega 2019, 4, 4129−4137

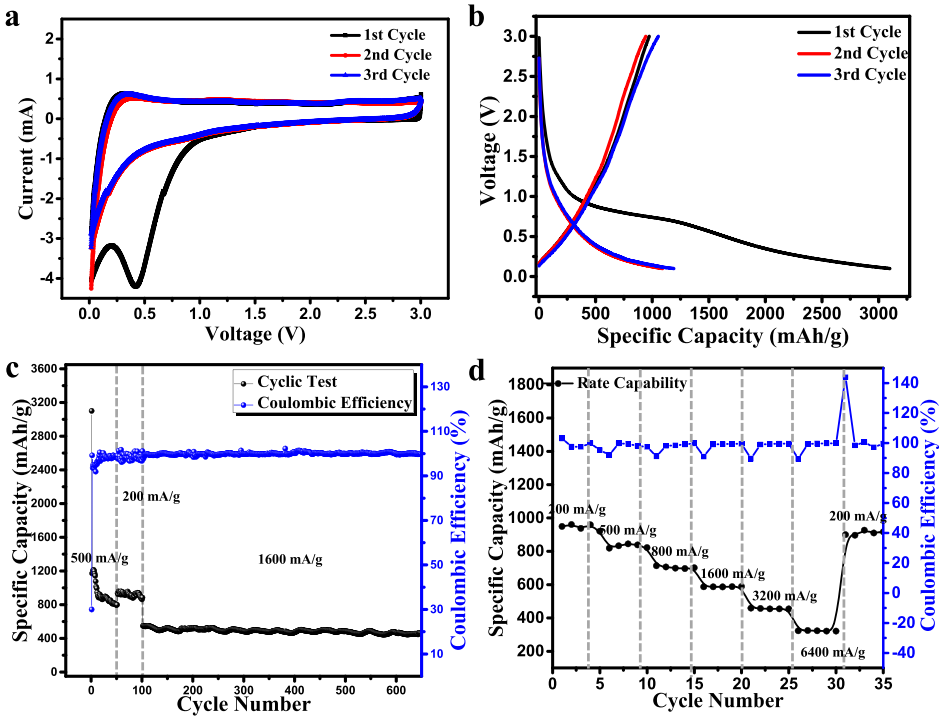

Figure 4. Electrochemical measurements for a PP-CNT; (a) cyclic voltammetry curve (b) charge/discharge curves at 500 mA/g for the first three cycles; (c) cyclic performance for 675 cycles at 500, 200, and 1600 mA/g; and (d) rate capability at different current densities from 200 to 6400 mA/g.

performance of the anode material. As previously mentioned, carbon yield and the diameter of the nanofiber are important to maintain the integrity of the matrix and hold the CNT intact. At the same time, the degree of graphitization must also be optimized in such a way that high conductivity can be observed. The carbonization temperature of 800 °C was chosen as a trade-off between the nanofiber diameter and conductivity. According to previous reports, the nanofiber diameter decreases as carbonization temperature increases, whereas the conductivity increases with carbonization temperature.[38] Higher graphitization occurs in higher temperature and causes the formation of more graphitic sheets and these layers have good stacking, resulting in higher conductivity. However, the degradation of carbon becomes more prominent as the temperature increases and, thus, an optimum temperature of 800 °C was chosen to accommodate both good fiber diameter and conductivity.[39]

The electrochemical properties of the PP-CNT were investigated through a series of comprehensive electrochemical analyses. After assembling the coin cell, cyclic voltammetry was conducted to determine the behavior of the anode material against a Li metal as both the counter and reference electrodes. Figure 4a shows the first three cyclic voltammetry curves for PP-CNT. The graph shows a typical curve observed for carbonaceous material. The first curve consists of a broad peak at around 0.5−1.0 V and disappears at the second and third curves, indicating the formation of a solid-electrolyte interface (SEI) layer. Normally, this is indicated by a high irreversible capacity for the first few cycles during charge/discharge. Insertion of the Li^+ ion is denoted by the peak at ∼0 V. This is present throughout the cycles but diminishes only after the first cycle, which is attributed to the initial intercalation of Li^+ ions into the CNT material. Delithiation is represented by a very weak and broad anodic peak at approximately ∼1.0 V. Succeeding cycles exhibit similar and overlapping peaks and curves, which means that PP-CNT has excellent reversibility and cycling stability as an anode material for LIB application.[40] Figure 4b shows the galvanostatic charge/discharge profiles of 1st, 2nd, and 3rd cycles at 500 mA/g current density between 0.005 and 3.0 V. The initial discharge capacity of 3100 mA h/g was observed in the PP-CNT electrode followed by 1091 mA h/g charge capacity, with a Coulombic efficiency of 34.3%. The lower Coulombic efficiency is mainly attributed to the large surface area of the PP-CNT electrode. The initial capacity loss is mainly because of either the inability to remove the complete Li^+ ion inserted during the first discharge during following charging or reduction of electrolyte and formation of an SEI layer on the electrode surface.[41,42]

To better understand the behavior of the PP-CNT electrode under cycling mode with different current densities, it was tested for long-term cycling at current densities of 500, 200, and 1600 mA/g as shown in Figure 4c. Initially, the PP-CNT electrode cycled for 50 cycles at a 500 mA/g current density. From the cycling test, it is observed that during initial cycles the discharge capacity of the PP-CNT electrode decreased continuously and got stabilized after 13 cycles. Despite capacity decay during initial cycles, the discharge capacity can retain a value of 800 mA h/g after 50 cycles. Furthermore, the same cell was cycled at 200 mA/g for another 50 cycles and discharge capacity performance is depicted in Figures 4c and S4. Figure S5 clearly shows that the capacity is almost constant throughout the 50 cycles, showing better stability of material. The PP-CNT retained a discharge capacity of 960 mA h/g after 50 cycles with 99% Coulombic efficiency, when cycled at a current density of 200 mA/g. Finally, to check long-term stability at a high current density of 1600 mA/g, the same cell was cycled for 675 cycles as shown in Figure 4c. The performance of the PP-CNT was further evaluated in

DOI: 10.1021/acsomega.8b03073
ACS Omega 2019, 4, 4129−4137

comparison with the bare CNT and PP. In all cases, the PP-CNT outperformed the two former samples at 500 mA/g. Figure S6 shows the capacitance of all the individual material wherein the CNT had a relatively stable performance, whereas, on the other hand, PP exhibited a sudden drop in the capacitance before the 50th cycle. The performance of the materials in separate conditions proved to be inferior but a synergistic effect was observed with both improved capacitance and stability when a composite of the two was used as an anode material. The effect of combining both the structural reinforcement of the polymeric matrix to allow electrolyte absorption and preventing particle migration together with the conductivity and lithiation mechanism of the CNT resulted in a high-performance freestanding electrode.

The long-term cycling stability test reveals that even at a high current density of 1600 mA/g, the electrode retain capacity is 521 mA h/g, which is higher than the theoretical capacity of a commercial graphite electrode (372 mA h/g). The corresponding charge/discharge curves of the following cycling test at each of the separate current densities (200, 500, 1600 mA/g) are presented in Figure S8, exhibiting good stability throughout the experiment. Throughout all cycling tests, a Coulombic efficiency of above ∼97−99% was observed, indicative of the high reversibility of the electrode. The performance of the PP-CNT is excellent and even higher compared to previously reported literature for carbon-based materials that are listed in Table S1. The high electrochemical performance of the PP-CNT electrode was mainly attributed to the 3D structure of the electrode with high surface area, maintaining its structural integrity.

Furthermore, the high rate of electrochemical performance of the PP-CNT electrode was investigated by a multiple-step galvanostatic strategy and the results are shown in Figure 4d. Initially, the cell was cycled at 500 mA/g for 20 cycles in order to avoid the induced effect because of activation of the electrode. After that, five cycles were measured to evaluate the capacity of the electrode at different current densities from 200 to 6400 mA/g stepwise and then decreased back to 200 mA/g. The rate capability analysis shows stable capacity retention at each current density. The electrode displayed the discharge capacities of 960, 844, 698, 587, 455, 323, and 915 mA h/g at 200, 500, 800, 1600, 3200, 6400, and 200 mA/g, respectively. More importantly, when the current density was decreased back to 200 from 6400 mA/g, the Coulombic efficiency remained ∼97−99% with a high recorded capacitance of ∼915 mA h/g which is ∼95% of the initial capacitance (960 mA h/g), indicating the excellent rate capability. The corresponding charge/discharge curves for the current densities in this experiment are all provided in Figure S9. The high electrochemical performance of the PP-CNT electrode can be attributed to the advantages of high surface area with porous structures, which greatly enhance the diffusion kinetics and buffer the volumetric changes.

In order to analyze the morphology change after a long-term cycling test, the electrode was soaked in dimethyl carbonate (DMC) solvent for 10 h to remove the SEI layer and dried at 40 °C overnight. No obvious change was observed after long-term cycling of the PP-CNT electrode as shown in figure S7. The electrode shows the nanofibers with a rougher surface.

To further understand the behavior of the electrode material, the electrochemical impedance spectroscopy measurement was carried out. Figure 5a,b represents the Nyquist plots before and after the cycling test with the representative

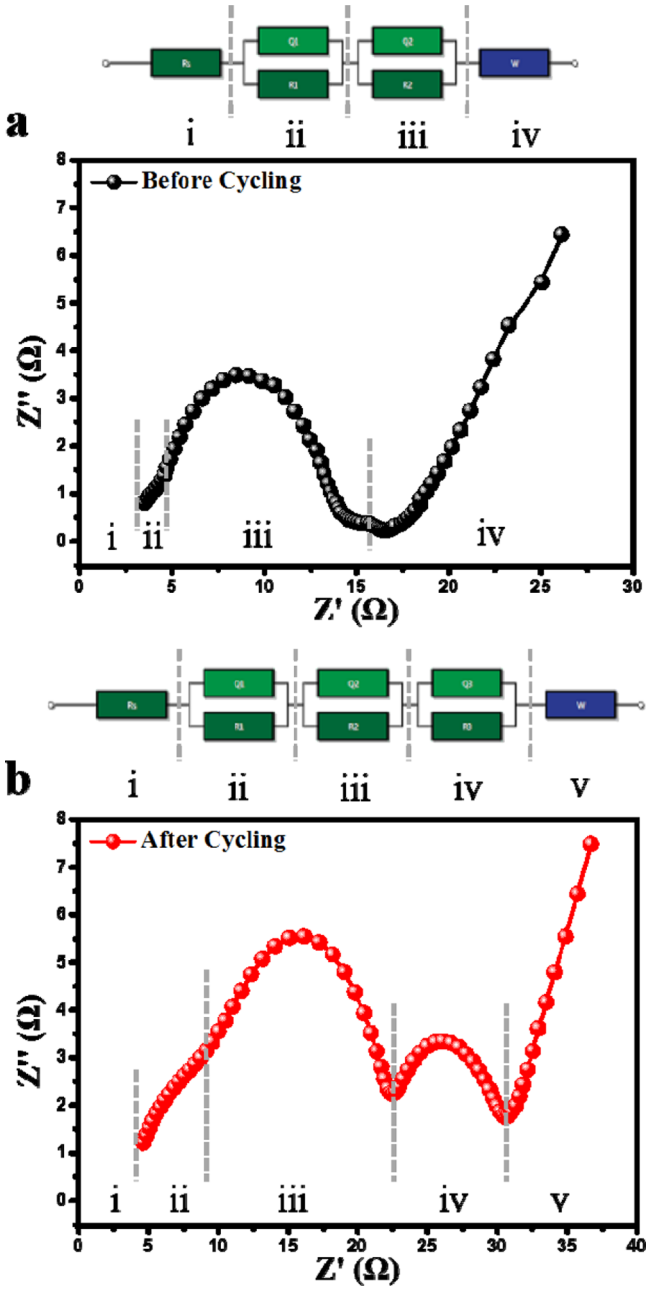

Figure 5. Nyquist plot of the PP-CNT before (a) and after 675 cycles (b).

electric circuit diagram. In Figure 5a, charge transfer resistance is the only prominent and observation curve followed by the diffusion curve at the low-frequency region. On the other hand, in Figure 5b, the plot is divided into 5 sections (i−v). Section (i) represents the electrolyte resistance, (ii,iii) appears to have an overlapped region between two semicircles, which is attributed to the surface film impedance (SEI layer) and the charge transfer resistance, which can be represented by (R_1||Q_1) and (R_2||Q_2) having resistance values of 17.5 and 7.77 Ω, respectively. The third semicircle at the lower frequency region is represented by (R_3||Q_3) attributed to Li^+ intercalation into the carbon, having a resistance value of 4.3 Ω.[43]

On the basis of the gathered results, it is found that PP-CNT is an excellent freestanding anode material used in a facile fabrication method consisting of electrospinning and pyrolysis

DOI: 10.1021/acsomega.8b03073
ACS Omega 2019, 4, 4129−4137

only. Moreover, a highly corrosive and toxic acidic oxidation step, typically employing CNT treatment for dispersion, was completely eliminated. As acidic oxidation can highly alter the intrinsic properties of a CNT, performance drop is mostly expected and stability can also pose problems. A good illustration of the advantages of a PP-CNT is shown in Scheme 2 wherein the polymer matrix serves a dual purpose.

Scheme 2. Illustration of Lithium Intercalation and CNT Stabilization

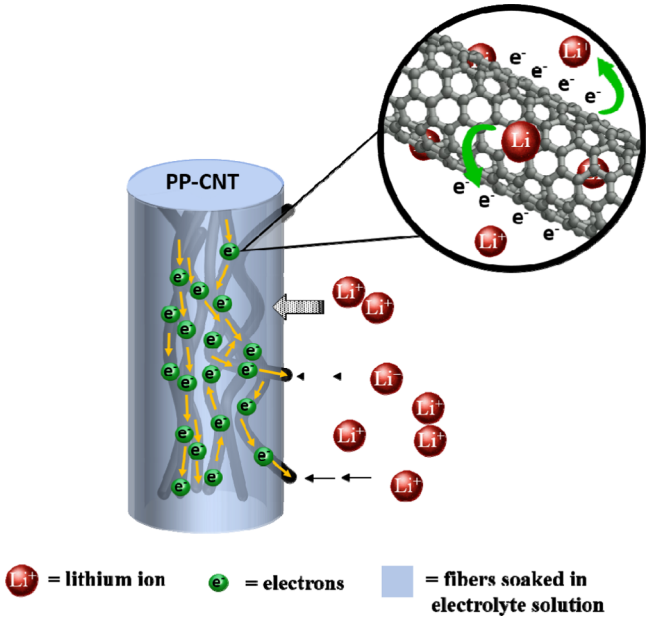

First, it provided the stability for CNT to prevent its migration, even at a high loading (ca. 50 wt %), and maintain its dispersed state by fixing them in a specific site within the bulk of the matrix. Second, it acts as an electrolyte reservoir that will preserve a consistent CNT−electrolyte interface throughout all processes. The lithium ions can both penetrate through the porous carbon and diffuse through the matrix or the lithium ions and can directly lithiate the CNT strands that are already slightly exposed from the surface of the nanofibers. Regardless, the lithium ions are facilitated to diffuse faster and maintain close proximity with the active site, preventing the agglomeration of CNTs and maintaining their well-dispersed arrangement by locking them in place, allowing for a more active site to be utilized during the charge/discharge process. The electrons flow through the CNT strands and extend out throughout the graphitized polymer matrix, creating a long-range conductivity to allow lithiation within the electrode material wherever lithium ions are present. Through this cooperative implementation of the stabilizing effect, a highly stable anode material was obtained. Thus, this study presents a method that can be highly attractive for practical applications and large-scale attempts.

In summary, a simple and safe fabrication of a PAN and PVP mixed polymer nanofiber with high CNT loading has been presented without the need of acidic oxidation to improve CNT dispersion in solution. A freestanding anode material (PP-CNT) was obtained after heat treatment and exhibited an outstanding lithium storage capacity of 960 mA h/g for more than 675 cycles at a high current density of 1600 mA/g with a consistent Coulombic efficiency of >95%. The rate capability experiment demonstrated the high reversibility of PP-CNT for a wide range of current densities and regaining >95% of its initial lithium storage capacity. The current study can be further extended for future development in LIBs and branch to other types of energy storage device applications.

EXPERIMENTAL PROCEDURE

Materials and Reagents. CNTs were provided by Samsung Company. PAN (average M_w 150 000) and PVP (average M_w 1 300 000) were purchased from Sigma-Aldrich. *N*,*N*′-Dimethyl formamide was purchased from Daejung Chemicals. All chemicals were of analytical reagent grade and commercially available, and used without further purifications. Deionized (D.I.) water was used throughout the experiments.

Fabrication of PP-CNT Nanofibers. CNTs (provided by Samsung) were ground and sieved (150 and 180 μm mesh size) properly before suspending in DMF solution. The CNTs were dispersed for 1 h using an ultrasonicator under an ice bath throughout the entire process. Subsequently, appropriate amounts of PAN and PVP were dissolved in the DMF solution to make a 10 wt % polymer solution with a 50 wt % CNT loading (based on the polymer amount). The mixture was heated to 50 °C and stirred overnight. The homogeneous solution was transferred into a polypropylene syringe with a 0.51 mm inner diameter needle tip. The syringe pump (model: EP100, NanoNC) flow rate was kept for 1 mL/h with an applied voltage (HV Power Supply, HV30, NanoNC) of 15−18 kV to form the nanofibers collected on an aluminum foil. The drum-type collector (model: DC90, NanoNC) and needle tip distance was 13 cm. The fabricated polymer fibers were vacuum-dried at 50 °C overnight. The polymer fibers were then subjected to thermal treatment at 280 °C at a ramping rate of 1 °C/min and held for 1 h. Then, the temperature was increased to 800 °C at a ramping rate of 5 °C/min and held for 1 h under nitrogen and cooled down to room temperature. The pyrolyzed polymer CNT nanofibers (denoted as PP-CNT in this paper) were used as desired.

Fabrication of Pyrolyzed PAN-PVP (PP). A similar procedure was conducted as mentioned above to fabricate pyrolyzed PAN-PVP without the loading of CNTs. Briefly, both PAN and PVP were dissolved in DMF to create a 10 wt % polymer solution. The mixture was stirred overnight at 50 °C to ensure the proper mixing and dissolution of the materials. The homogeneous solution was transferred into a polypropylene syringe with a 0.51 mm inner diameter needle tip. The syringe pump (model: EP100, NanoNC) flow rate was kept at 1 mL/h with an applied voltage (HV Power Supply, HV30, NanoNC) of 15−18 kV to form the nanofibers collected on an aluminum foil. The drum-type collector (model: DC90, NanoNC) and needle tip distance was 13 cm. The fabricated polymer fibers were vacuum-dried at 50 °C overnight. The polymer fibers were then subjected to thermal treatment at 280 °C at a ramping rate of 1 °C/min and held for 1 h. Then, the temperature was increased to 800 °C at a ramping rate of 5 °C/min and held for 1 h under nitrogen and cooled down to room temperature. The nanofiber material obtained was labeled as PP.

Fabrication of the CNT Electrode. The CNT electrode was prepared by mixing CNT and poly(vinylidene difluoride) (at a weight ratio of 80:20) in *N*-methyl-2-pyrrolidone to create a paste-like solution. This was uniformly spread on a copper foil, as the current collector, using an automatic control

DOI: 10.1021/acsomega.8b03073
ACS Omega 2019, 4, 4129−4137

coater. The material was dried at 80 °C overnight to completely remove the moisture and residual solvents. Afterward, the prepared electrodes were punched into circular discs and used as anode material to assemble coin cells for electrochemical measurement.

Material Characterization. The phase and morphology of the material were characterized by a powder X-ray diffractometer (Shimadzu XRD-6000) with Cu Kα irradiation (λ = 1.5406 Å); field emission SEM (FE-SEM, Sigma S-4000) for the morphological studies and infrared spectra of the prepared the electrodes were obtained using FT-IR spectroscopy (Agilent, Cary 630). Raman spectra were recorded on a Photon Design spectrometer using an argon ion laser with an excitation wavelength of 514 nm. The specific surface area and pore size distribution of the materials were all studied by a BELSORP-miniII (BEL, Japan) instrument with the method of BET and micropore analysis for surface area and pore size distribution analysis, respectively. Prior to the actual absorption experiment, the samples were degassed at 100 °C for 12 h.

Electrochemical Measurement. All electrochemical measurements were executed using coin-type 2032 cells. To prepare working electrodes, the as-prepared active materials (50 wt % CNT pyrolyzed nanofibers) were punched into circular discs and electrochemical measurements of the electrode materials were carried out using a coin-type half-cell (2032) assembled in an Ar-filled glove box with lithium metal as a counter electrode and glass fiber, soaked with $LiPF_6$ in ethylene carbonate and DMC (1:1, by volume), as the separator. The electrochemical tests of the electrode were investigated by performing cyclic voltammogram measurements at a scan rate of 0.05 mV/s in the voltage range of 0−3.0 V (vs Li/Li^+) using the Won-A-Tech potentiostat/galvanostatic instrument at 25 °C. Furthermore, the cells were galvanostatically discharge−charged between 0.005 and 3.0 V versus Li/Li^+ using a Won-A-Tech battery cycler. The impendence spectra of the assembled half-cells were recorded with an amplitude of 10 mV over a frequency range from 1 Hz to 1 MHz using the ZIVE SP2 instrument. All electrochemical tests were conducted at 25 °C.

■ ASSOCIATED CONTENT

Supporting Information

The Supporting Information is available free of charge on the ACS Publications website at DOI: 10.1021/acsomega.8b03073.

Additional characterization analyses such as FT-IR, XRD, Raman spectroscopic analysis, and thermal gravimetric (TG) decomposition analysis; bode plot and electrochemical performance comparison from previous reported literature (PDF)

■ AUTHOR INFORMATION

Corresponding Author

*E-mail: jgseo@mju.ac.kr (J.G.S.).

ORCID

Hyuk Jae Kwon: 0000-0002-7915-1383

Jeong Gil Seo: 0000-0002-3166-3590

Author Contributions

§A.C.L. and H.S.J. equally contributed in this work.

Notes

The authors declare no competing financial interest.

■ ACKNOWLEDGMENTS

This work was supported by the National Research Foundation of Korea (NRF) funded by the Ministry of Science, ICT and Future Planning (NRF-2016R1C1B2008694). This work was also supported by Nano-Material Fundamental Technology Development (2016M3A7B4909370) through the National Research Foundation of Korea (NRF) funded by the Ministry of Science, ICT, and Future Planning. This work was financially supported by Samsung Advanced Institute of Technology, Samsung Electronics Co., Ltd.

■ REFERENCES

(1) Rodrigues, M.-T. F.; Babu, G.; Gullapalli, H.; Kalaga, K.; Sayed, F. N.; Kato, K.; Joyner, J.; Ajayan, P. M. A Materials Perspective on Li-Ion Batteries at Extreme Temperatures. *Nat. Energy* **2017**, *2*, 17108.

(2) Scrosati, B. Challenge of Portable Power. *Nature* **1995**, *373*, 557−558.

(3) Nan, D.; Huang, Z.-H.; Lv, R.; Yang, L.; Wang, J.-G.; Shen, W.; Lin, Y.; Yu, X.; Ye, L.; Sun, H.; Kang, F. Nitrogen-enriched electrospun porous carbon nanofiber networks as high-performance free-standing electrode materials. *J. Mater. Chem. A* **2014**, *2*, 19678−19684.

(4) Li, H.; Wang, Z.; Chen, L.; Huang, X. Research on Advanced Materials for Li-Ion Batteries. *Adv. Mater.* **2009**, *21*, 4593−4607.

(5) Li, J.; Klee Barillas, J.; Guenther, C.; Danzer, M. A. A comparative study of state of charge estimation algorithms for $LiFePO_4$ batteries used in electric vehicles. *J. Power Sources* **2013**, *230*, 244−250.

(6) Winter, M.; Brodd, R. J. What Are Batteries, Fuel Cells, and Supercapacitors? *Chem. Rev.* **2004**, *104*, 4245−4270.

(7) Skea, J.; Nishioka, S. Policies and Practices for a Low-Carbon Society. *Clim. Pol.* **2008**, *8*, S5−S16.

(8) Wang, S.-X.; Chen, S.; Wei, Q.; Zhang, X.; Wong, S. Y.; Sun, S.; Li, X. Bioinspired Synthesis of Hierarchical Porous Graphitic Carbon Spheres with Outstanding High-Rate Performance in Lithium-Ion Batteries. *Chem. Mater.* **2014**, *27*, 336−342.

(9) Goriparti, S.; Miele, E.; De Angelis, F.; Di Fabrizio, E.; Proietti Zaccaria, R. Review on Recent Progress of Nanostructured Anode Materials for Li-Ion Batteries. *J. Power Sources* **2014**, *257*, 421−443.

(10) Cheng, C.; Fan, R.; Wang, Z.; Shao, Q.; Guo, X.; Xie, P.; Yin, Y.; Zhang, Y.; An, L.; Lei, Y.; Ryu, J. E.; Shankar, A.; Guo, Z. Tunable and weakly negative permittivity in carbon/silicon nitride composites with different carbonizing temperatures. *Carbon* **2017**, *125*, 103−112.

(11) Zhang, Q.; Gao, Q.; Qian, W.; Zhang, H.; Tan, Y.; Tian, W.; Li, Z.; Xiao, H. Graphene-based Carbon Coated Tin Oxide as a Lithium Ion Battery Anode Material with High Performance. *J. Mater. Chem. A* **2017**, *5*, 19136−19142.

(12) Wang, S.; Wang, R.; Chang, J.; Hu, N.; Xu, C. Self-supporting Co_3O_4/Graphene Hybrid Films as Binder-free Anode Materials for Lithium Ion Batteries. *Sci. Rep.* **2018**, *8*, 3182.

(13) Xu, C.; Niu, D.; Zheng, N.; Yu, H.; He, J.; Li, Y. Facile Synthesis of Nitrogen-Doped Double-Shelled Hollow Mesoporous Carbon Nanospheres as High-Performance Anode Materials for Lithium Ion Batteries. *ACS Sustainable Chem. Eng.* **2018**, *6*, 5999−6007.

(14) Yang, Y.; Jin, S.; Zhang, Z.; Du, Z.; Liu, H.; Yang, J.; Xu, H.; Ji, H. Nitrogen-Doped Hollow Carbon Nanospheres for High-Performance Li-Ion Batteries. *ACS Appl. Mater. Interfaces* **2017**, *9*, 14180−14186.

(15) Fang, Y.; Lv, Y.; Che, R.; Wu, H.; Zhang, X.; Gu, D.; Zheng, G.; Zhao, D. Two-dimensional Mesoporous Carbon Nanosheets and their

DOI: 10.1021/acsomega.8b03073
ACS Omega 2019, 4, 4129−4137

derived Graphene Nanosheets: Synthesis and Efficient Lithium Ion Storage. *J. Am. Chem. Soc.* **2013**, *135*, 1524−1530.
(16) Song, R.; Song, H.; Zhou, J.; Chen, X.; Wu, B.; Yang, H. Y. Hierarchical Porous Carbon Nanosheets and their Favorable High-rate Performance in Lithium Ion Batteries. *J. Mater. Chem.* **2012**, *22*, 12369−12374.
(17) de las Casas, C.; Li, W. A review of application of carbon nanotubes for lithium ion battery anode material. *J. Power Sources* **2012**, *208*, 74−85.
(18) Lin, C.; Hu, L.; Cheng, C.; Sun, K.; Guo, X.; Shao, Q.; Li, J.; Wang, N. Nano-$TiNb_2O_7$/carbon nanotubes composite anode for enhanced lithium-ion storage. *Electrochim. Acta* **2018**, *260*, 65−72.
(19) Zhao, T.; She, S.; Ji, X.; Jin, W.; Dang, A.; Li, H.; Li, T.; Shang, S.; Zhou, Z. In-situ Growth Amorphous Carbon Nanotube on Silicon Particles as Lithium-Ion Battery Anode Materials. *J. Alloys Compd.* **2017**, *708*, 500−507.
(20) Di Lecce, D.; Andreotti, P.; Boni, M.; Gasparro, G.; Rizzati, G.; Hwang, J.-Y.; Sun, Y.-K.; Hassoun, J. Multiwalled Carbon Nanotubes Anode in Lithium-Ion Battery with $LiCoO_2$, $Li[Ni_{1/3}Co_{1/3}Mn_{1/3}]O_2$, and $LiFe_{1/4}Mn_{1/2}Co_{1/4}PO_4$ Cathodes. *ACS Sustainable Chem. Eng.* **2018**, *6*, 3225−3232.
(21) Ventrapragada, L. K.; Zhu, J.; Creager, S. E.; Rao, A. M.; Podila, R. A Versatile Carbon Nanotube-Based Scalable Approach for Improving Interfaces in Li-Ion Battery Electrodes. *ACS Omega* **2018**, *3*, 4502−4508.
(22) Gao, H.; Xin, S.; Xue, L.; Goodenough, J. B. Stabilizing a High-Energy-Density Rechargeable Sodium Battery with a Solid Electrolyte. *Chem* **2018**, *4*, 833−844.
(23) Gao, H.; Xue, L.; Xin, S.; Goodenough, J. B. A High-Energy-Density Potassium Battery with a Polymer-Gel Electrolyte and a Polyaniline Cathode. *Angew. Chem., Int. Ed.* **2018**, *57*, 5449−5453.
(24) Gao, H.; Xue, L.; Xin, S.; Park, K.; Goodenough, J. B. A Plastic-Crystal Electrolyte Interphase for All-Solid-State Sodium Batteries. *Angew. Chem., Int. Ed.* **2017**, *56*, 5541−5545.
(25) Xie, X.; Mai, Y.; Zhou, X. Dispersion and alignment of carbon nanotubes in polymer matrix: A review. *Mater. Sci. Eng., R* **2005**, *49*, 89−112.
(26) Salim, N. V.; Blight, S.; Creighton, C.; Nunna, S.; Atkiss, S.; Razal, J. M. The Role of Tension and Temperature for Efficient Carbonization of Polyacrylonitrile Fibers: Toward Low Cost Carbon Fibers. *Ind. Eng. Chem. Res.* **2018**, *57*, 4268−4276.
(27) Zhang, B.; Kang, F.; Tarascon, J.-M.; Kim, J.-K. Recent Advances in Electrospun Carbon nanofibers and their Application in Electrochemical Energy Storage. *Prog. Mater. Sci.* **2016**, *76*, 319−380.
(28) Guangzhi, Y.; Binbin, Y.; Shen, S.; Zhihong, T.; Dengguang, Y.; Junhe, Y. Preparation and dispersity of Carbon Nanospheres by Carbonizing Polyacrylonitrile Microspheres. *RSC Adv.* **2017**, *7*, 16341−16347.
(29) Maddah, B.; Soltaninezhad, M.; Adib, K.; Hasanzadeh, M. Activated carbon nanofiber produced from electrospun PAN nanofiber as a solid phase extraction sorbent for the preconcentration of organophosphorus pesticides. *Separ. Sci. Technol.* **2016**, *52*, 700−711.
(30) Ding, Y.; Wang, Y.; Su, L.; Bellagamba, M.; Zhang, H.; Lei, Y. Electrospun Co_3O_4 nanofibers for sensitive and selective glucose detection. *Biosens. Bioelectron.* **2010**, *26*, 542−548.
(31) Liu, C.; Sergeichev, I.; Akhatov, I.; Lafdi, K. CNT and polyaniline based sensors for the detection of acid penetration in polymer composite. *Compos. Sci. Technol.* **2018**, *159*, 111−118.
(32) Al-Attabi, R.; Dumée, L. F.; Kong, L.; Schütz, J. A.; Morsi, Y. High Efficiency Poly(acrylonitrile) Electrospun Nanofiber Membranes for Airborne Nanomaterials Filtration. *Adv. Eng. Mater.* **2017**, *20*, 1700572.
(33) Xia, H.; Wang, Y.; Lin, J.; Lu, L. Hydrothermal Synthesis of MnO_2/CNT Nanocomposite with a CNT core/porous MnO_2 Sheath Hierarchy Architecture for Supercapacitors. *Nanoscale Res. Lett.* **2012**, *7*, 33.
(34) Chaikittisilp, W.; Hu, M.; Wang, H.; Huang, H.-S.; Fujita, T.; Wu, K. C.-W.; Chen, L.-C.; Yamauchi, Y.; Ariga, K. Nanoporous Carbons through Direct Carbonization of a Zeolitic Imidazolate Framework for Supercapacitor Electrodes. *Chem. Commun.* **2012**, *48*, 7259−7261.
(35) Scaffaro, R.; Maio, A.; Tito, A. C. High Performance PA_6/CNTs Nanohybrid Fibers Prepared in the Melt. *Compos. Sci. Technol.* **2012**, *72*, 1918−1923.
(36) Yang, X.; Yu, M.; Zhao, Y.; Zhang, C.; Wang, X.; Jiang, J.-X. Remarkable gas adsorption by carbonized nitrogen-rich hypercrosslinked porous organic polymers. *J. Mater. Chem. A* **2014**, *2*, 15139−15145.
(37) Li, W.; Zhang, L.-S.; Wang, Q.; Yu, Y.; Chen, Z.; Cao, C.-Y.; Song, W.-G. Low-cost Synthesis of Graphitic Carbon Nanofibers as Excellent Room Temperature Sensors for Explosive Gases. *J. Mater. Chem.* **2012**, *22*, 15342−15347.
(38) Lee, H.-M.; An, K.-H.; Kim, B.-J. Effects of carbonization temperature on pore development in polyacrylonitrile-based activated carbon nanofibers. *Carbon Lett.* **2014**, *15*, 146−150.
(39) Panapoy, M.; Dankeaw, A.; Ksapabutr, B. Electrical Conductivity of PAN-based Carbon Nanofibers Prepared by Electrospinning Method. *Int. J. Sci. Technol.* **2008**, *13*, 11−17.
(40) Chen, C.; Agrawal, R.; Hao, Y.; Wang, C. Activated Carbon Nanofibers as High Capacity Anodes for Lithium-Ion Batteries. *ECS J. Solid State Sci. Technol.* **2013**, *2*, M3074−M3077.
(41) Jadhav, H. S.; Thorat, G. M.; Mun, J.; Seo, J. G. Self-assembled hierarchical 3D - NiO microspheres with ultra-thin porous nanoflakes for lithium-ion batteries. *J. Power Sources* **2016**, *302*, 13−21.
(42) Jadhav, H. S.; Rai, A. K.; Lee, J. Y.; Kim, J.; Park, C.-J. Enhanced electrochemical performance of flower-like Co_3O_4 as an anode material for high performance lithium-ion batteries. *Electrochim. Acta* **2014**, *146*, 270−277.
(43) Wang, L.; Zhao, J.; He, X.; Gao, J.; Li, J.; Wan, C.; Jiang, C. Electrochemical Impedance Spectroscopy (EIS) Study of $LiNi_{1/3}Co_{1/3}Mn_{1/3}O_2$ for Li-Ion Batteries. *Int. J. Electrochem. Sci.* **2012**, *7*, 345−353.

DOI: 10.1021/acsomega.8b03073
ACS Omega 2019, 4, 4129−4137